Compressive strength degradation in ZrB2-based ultra-high temperature ceramic composites

J. Ramírez-Rico (a) , M.A. Bautista (a), J. Martínez-Fernández (a), M. Singh (b)

a Dpto. Física de la Materia Condensada-ICMSE, Universidad de Sevilla-CSIC, Avda. Reina Mercedes s/n, 41012 Sevilla, Spain

b Ohio Aerospace Institute. NASA Glenn Research Center, Cleveland, OH 44135-3191, USA

Abstract

The high temperature compressive strength behavior of zirconium diboride (ZrB2)–silicon carbide (SiC) particulate composites containing either carbon powder or SCS-9a silicon carbide fibers was evaluated in air. Constant strain rate compression tests have been performed on these materials at room temperature, 1400, and 1550 °C. The degradation of the mechanical properties as a result of atmospheric air exposure at high temperatures has also been studied as a function of exposure time. The ZrB2–SiC material shows excellent strength of 3.1 ± 0.2 GPa at room temperature and 0.9 ± 0.1 GPa at 1400 °C when external defects are eliminated by surface finishing. The presence of C is detrimental to the compressive strength of the ZrB2–SiC–C material, as carbon burns out at high temperatures in air. As-fabricated SCS-9a SiC fiber reinforced ZrB2–SiC composites contain significant matrix microcracking due to residual thermal stresses, and show poor mechanical properties and oxidation resistance. After exposure to air at high temperatures an external SiO2 layer is formed, beneath which ZrB2 oxidizes to ZrO2. A significant reduction in room temperature strength occurs after 16–24 h of exposure to air at 1400 °C for the ZrB2–SiC material, while for the ZrB2–SiC–C composition this reduction is observed after less than 16 h. The thickness of the oxide layer was measured as a function of exposure time and temperatures and the details of oxidation process has been discussed.

Keywords

Composites; Borides; Carbides; Strength; Structural applications

1. Introduction

The high melting point of refractory metal diborides coupled with their ability to form refractory oxide scales give these materials the capacity to withstand temperatures in the 1900–2500 °C range. These ultra-high temperature ceramics (UHTCs) were developed in the 1960s. [1] Fenter [2] provided a comprehensive review of the work accomplished in the 1960s and early 1970s. These materials are almost never used in

pure form. Instead, additions of silicon carbide are used to enhance oxidation resistance and limit diboride grain growth. [3], [4], [5] and [6] Carbon is also sometimes used as an additive to enhance thermal stress resistance. [7], [8] and [9] These materials offer a good combination of properties that make them candidates for airframe leading edges on sharp bodied re-entry vehicles. [10] UHTCs have potential to perform well in such applications' environment, i.e. air at low pressure. Some interest has also been shown in these materials for single use propulsion applications.[11]

Major improvements in the manufacturing and characterization of ZrB2 materials and composites have been put forward in recent years, and now several important aspects of their properties and processing are well understood. [4], [12], [13], [14], [15], [16], [17], [18], [19], [20] and [21] However, the study of high temperature properties has been mostly limited to oxidation behavior, an area which is also well understood. [8], [21], [22], [23], [24], [25], [26], [27] and [28] Very few studies of high temperature mechanical properties exist. [7], [11] and [29]

In this work, we investigated the mechanical behavior of ZrB2–SiC composites, with and without added C and SCS-9a fibers. Samples were studied in compression at room temperature, 1400, and 1550 °C, in atmospheric air. The degradation of the mechanical properties as a result of atmospheric air exposure at high temperatures were also studied as a function of exposure time.

2. Experimental procedures

Samples of ZrB2–SiC composites were fabricated by uniaxial hot pressing by Materials and Machines, Inc., Tucson, AZ. ZrB2 and α-SiC powders were obtained from H. C. Starck and had nominal sizes of d50 = 3–5 μm and d50 = 1.4 μm, respectively. C powders were obtained from Asbury Graphite Mills. SiC fibers were obtained from Textron Specialty Materials (SCS-9a fibers). Two particulate composites were studied, one containing ZrB2 plus 20 vol.% SiC (ZS), and the other containing ZrB2 plus 14 vol.% SiC and 30 vol.% C (ZSC). The specimen densities obtained were 5.57 g/cm3 (99.9% of theoretical density) for ZS and 4.50 g/cm3 (99.0% of theoretical density) for ZSC. The composite panel was prepared by the filament winding and slurry deposition technique followed by hot pressing in a graphite die. The composite density obtained was 3.47 g/cm3, while the theoretical density is 4.60 g/cm3 for 35 vol.% fiber loading.

Compression tests were carried out on an electromechanical universal testing machine with a furnace attached to its frame, at constant cross-head displacement rate (strain rates of 2 × 10−5 s−1 and 2 × 10−4 s−1). Load was applied using alumina rods with SiC pads. Samples were cut into parallelepiped shape using a low speed diamond saw. Nominal sample dimensions were 3 mm × 3 mm × 5 mm, and the load was applied to the longest dimension. Some samples were finely polished (up to 0.5 μm) to further study the strength dependence with surface defects. Mechanical tests were conducted

at room temperature, 1400, and 1550 °C. Several samples were exposed to oxidation by annealing at 1400 °C in atmospheric air in a tube furnace, and exposure times ranged from 6 to 48 h. The room temperature strength was measured after oxidation, to study the degradation of the mechanical properties after exposure to an oxidizing environment. At least three samples were studied at each temperature or exposure time at 1400 °C. Error bars throughout this paper represent one standard deviation.

Microstructural studies were carried out using SEM and EDS techniques, on both as-fabricated and tested specimens. Samples were prepared for SEM observation using conventional metallographic techniques which involved cutting, grinding, and lapping. A conductive coating of either carbon or gold was applied to the specimens prior to microscopic observation.

3. Results and discussion

3.1. Microstructure of as-received specimens

Fig. 1 shows the as-fabricated microstructures of three types of composites studied. The ZS composite appears to be fully dense, while the ZSC suffered from significant grain pullout during sample preparation. This is attributed to the weak bonding of C to the ZrB2 and SiC phases, which results in removal of the C phase during polishing. In ZS, ZrB2 grains (gray phase) are equiaxed with reported grain size in the 6–12 μm range, while the SiC grains (dark phase) are elongated with sizes of approximately 1.5–3 μm thick by 3–11 μm wide/long. [7] In ZSC, the grain pullout during polishing made the estimation of grain size difficult, although it can be seen from Fig. 1 that ZrB2 grain size is smaller in ZSC than in ZS. It should be noted that, at least for the ZS composite, the grain size is close to the critical grain size for microcracking due to the anisotropic thermal expansion coefficient of ZrB2, which has been reported to be around 15 μm.30

The fiber composite microstructure is shown in Fig. 1C and D. Fibers were distributed in layers, and regularly spaced matrix cracking is produced due to residual thermal stresses that appear because of the differences in thermal expansion coefficients of the fibers and the matrix. A detailed view is presented in Fig. 2, which also shows that significant amount of porosity is present in the matrix. Fig. 3 shows elemental maps of the ZSS composite obtained by EDS. It can be seen that the SCS-9a fibers contain a carbon core surrounded by SiC. From Fig. 1 and Fig. 3 it can be concluded that the fiber coating remained intact during the uniaxial pressing step of the fabrication route.

3.2. Room and high temperature strength

The compressive strength was measured at room temperature, 1400, and 1550 °C in atmospheric air for the ZS, ZSC, and ZSS composites. Fig. 4 shows representative room temperature stress–strain curves for the compositions, strain rates, and surface

finishing studied. Note that due to the large differences measured in strength, the stress–strain curves are plotted in a semilogarithmic scale.

No strain rate dependence was observed for the room temperature strength in the strain rate range of 2 × 10−5 s−1 to 2 × 10−4 s−1, as can be seen in the stress–strain curves of ZS and ZSC materials (Fig. 4). This is typical of defect-controlled strength situation in which defects act as stress concentrators nucleating cracks and failure. Average compression strength of 3.1 ± 0.2 GPa were measured for ZS versus the 0.88 ± 0.08 GPa strength obtained for the ZS unpolished samples. For ZSC the average compression strength of 560 ± 80 MPa was measured for the finely polished samples and average compression strength of 630 ± 50 MPa was obtained for the ZSC unpolished samples, implying that internal instead of external defects are responsible for fracture. It is clear that ZS materials have exceptionally high intrinsic strength, which is limited by fabrication or finishing defects. In the case of the ZSC material the carbon regions act as flaws for crack nucleation and the finish of the external surface is not a limiting factor in strength.

Fig. 5A shows a general view of the fracture surface microstructure of a ZS sample that failed at 3.2 GPa. It is clear from the figure that the ZrB2 failure is transgranular, while SiC grains are pulled out at the fracture surface and therefore remain intact. In Fig. 5B a higher magnification detail of the fracture surface is presented, where presence of intergranular small cracks can be noticed. It is interesting to note that the stress–strain curves are not linear at high stresses (Fig. 4), indicating that the microstructure is changing due to the generation of internal defects until they reach the critical size for failure.

Typical stress–strain curves of ZSS along directions parallel and perpendicular to the fibers are also shown in Fig. 4. Measured strengths were 330 ± 150 and 240 ± 30 MPa for samples loaded parallel and perpendicular to the fibers, respectively. The compression strength is controlled by the penny-shaped cracks formed during the sintering step and therefore is higher when the fibers are parallel to the compression direction, as in that case the cracks are perpendicular to the applied load.

Representative high temperature stress–displacement curves are shown in Fig. 6 for materials tested at 1400, and 1550 °C. Fig. 7 summarizes the results obtained, and shows the average compressive strength as a function of temperature. Surface defects are seen to play an important role in limiting the compressive strength of ZS materials up to 1400 °C, while at 1550 °C the measured strength is similar for polished and unpolished samples, implying that oxidation effects are dominant at these temperatures. In general, the ZS composite shows higher compressive strength than the carbon containing ZSC. This is attributed to both the weak carbon bonding to the other phases, evidenced as grain pullout in the SEM observations, and the burnout of carbon at high temperature in air. This creates porosity and also produces channels

through which air can enter, oxidizing the ZrB2 phase not only on the surface but also inside the sample.

Plastic deformation is clear in ZS and ZSC materials at 1400, and 1550 °C. The ZS materials can undergo substantially more strain than ZSC materials, because grains start loosing contact points earlier in ZSC due to the initial porosity associated to carbon burnout. Plastic deformation must be associated to grain boundary sliding, because of the high intrinsic strength and low diffusion coefficient of ZrB2. Grain boundary sliding is however difficult by the lack of intergranular phases and the presence of smaller SiC grains the boundaries and triple points.

The extensive cracking in ZSS causes very poor high temperature behavior. At high temperature, cracks cause extensive oxidation through the sample and elimination of the fibers' coating (Fig. 8). The high temperature strength is therefore very low compared to ZS and ZSC composites.

3.3. Oxidation and strength degradation

The ZS and ZSC composites were selected for the study of strength degradation at high temperature. The degradation in the mechanical properties was studied as a function of exposure time to atmospheric air at 1400 °C. These results are summarized in Fig. 9, where the room temperature strength of the materials is plotted as a function of exposure time. For ZS, a reduction of 33% in strength occurred between 16 and 24 h, while for ZSC less than 16 h were needed. This can be explained considering that C burns in the oxidizing atmosphere, creating pores and channels through which air can permeate.

The microstructure and thickness of the oxide layers formed after exposure to atmospheric air at 1400 °C was studied for both ZS and ZSC samples, which were cut and polished for observation in the SEM. Fig. 10(left) shows a micrograph and compositional maps for a ZS sample annealed for 1 h. The outer, Si and O rich layer can be concluded to be SiO2, while the intermediate layer, which is O rich and B poor, is ZrO2. Similar conclusions can be drawn from Fig. 12(right), which represents compositional maps for a ZSC sample annealed for 24 h. Again, the outer layer is mainly composed of SiO2, and an intermediate layer of ZrO2 separates the former layer and the bulk interior of the sample.

These observations were confirmed by quantitative analysis, of which an example is presented. Fig. 11 is a cross section of a ZSC sample annealed for 24 h at 1400 °C in air, and contains several of the features previously observed. The microstructure of the oxide layer can be divided into four different zones or regions. The first, outer one is composed of ZrO2 grains embedded in a glassy SiO2 matrix, as can be deduced from the elemental composition. The zone labeled as number 2 is composed only of SiO2, while the zone labeled as 3 is composed almost exclusively of ZrO2 and contains no Si.

The fourth zone corresponds to the composition of the bulk, as-fabricated material. For ease of comparison, raw spectra obtained from all four different zones are depicted.

These observations confirm the oxidation process already outlined in previous references, such as Refs. [7], [8], [25], [26] and [28]. Both ZrB2 and SiC are oxidized, producing B2O3 that evaporates at high temperatures. The SiO2 formed, which is liquid at the studied conditions, is expelled towards the surface of the sample by capillary forces, and acts as a protective layer. The intermediate layer is thus composed mostly of ZrO2 and pores that allow for oxygen permeation. It is thus expected that the ZSC samples, containing carbon that burns out at high temperature, will oxidize at a faster rate because of the porosity produced during carbon combustion.

To ascertain this effect, the thickness of both the SiO2 and ZrO2 oxide layers were measured as a function of annealing time, for both ZS and ZSC samples. These results are presented in Fig. 12. ZS material shows an increase of the oxide layer as , typical of diffusion controlled process. This is expected as oxygen diffusion trough the SiO2 layer, in either molecular or atomic form, is necessary to further increase the oxide layer thickness.

In the ZSC material the carbon readily burns out, creating channels and a rapid formation of a thick SiO2 layer. Once the initial SiO2 layer (with thickness of approximately 50 μm) is formed, the process is controlled by oxygen diffusion and the thickness increase of the reaction layer can be fit as , typical of diffusion process in which an initial condition exists. The good fit to the experimental data shown in Fig. 12 supports the hypothesis of a diffusion controlled oxidation process.

4. Conclusions

The ZrB2–SiC composition shows the best performance of the three materials studied, both in terms of strength and oxidation resistance. This material presents an exceptional room temperature compressive strength of 3.1 ± 0.2 GPa and a high temperature strength of 0.9 ± 0.1 GPa at 1400 °C, and can withstand exposures up to 24 h in air at 1400 °C before its compressive strength falls significantly when compared to the as-fabricated material.

It has been shown that the addition of C to a ZrB2–SiC composite is detrimental to the high temperature mechanical properties, since the degradation in strength and oxidation resistance observed counters any possible improvement to the thermal shock resistance. The ZrB2–SiC–C composition is probably not suitable for application in air if no protective coating is applied. The oxidation process has been shown to be diffusion controlled and the application of a diffusional barrier is probably needed.

As-fabricated SCS-9a SiC fiber reinforced ZrB2 presents significant matrix microcracking due to residual thermal stresses, and therefore shows poor mechanical properties and oxidation resistance.

Acknowledgements

This material is based upon work supported by the European Office of Aerospace Research and Development, Air Force Office of Scientific Research, Air Force Research Laboratory, under Grant No. FA8655-07-1-3087. Any opinions, findings and conclusions or recommendations expressed in this material are those of the authors and do not necessarily reflect the views of the European Office of Aerospace Research and Development, Air Force Office of Scientific Research or Air Force Research Laboratory. SEM observations were done at the CITIUS of the Universidad de Sevilla. J.R.-R. was funded by a Junta de Andalucía FPDI grant.

References

1. E.V. Clougherty, R.L. Pober, L. Kaufman

Synthesis of oxidation resistant metal diboride composites

Trans Met Soc AIME, 242 (1968), pp. 1077–1082

2. J.R. Fenter

Refractory diborides as engineering materials

SAMPE Quart, 2 (1971), pp. 1–15

3. G.J. Zhang, Z.Y. Deng, N. Kondo, J.F. Yang, T. Ohji

Reactive hot pressing of ZrB2–SiC composites

J Am Ceram Soc, 83 (2000), pp. 2330–2332

4. F. Monteverde

Beneficial effects of an ultra-fine α-SiC incorporation on the sinterability and mechanical properties of ZrB2

Appl Phys A-Mater, 82 (2006), pp. 329–337

5. Y. Yan, Z. Huang, S. Dong, D. Jiang

Pressureless sintering of high-density ZrB2–SiC ceramic composites

J Am Ceram Soc, 89 (2006), pp. 3589–3592

6. S. Zhu, W.G. Fahrenholtz, G.E. Hilmas

Influence of silicon carbide particle size on the microstructure and mechanical properties of zirconium diboride–silicon carbide ceramics

J Eur Ceram Soc, 27 (2007), pp. 2077–2083

7. S.R. Levine, E.J. Opila, M.C. Halbig, J.D. Kiser, M. Singh, J.A. Salem

Evaluation of ultra-high temperature ceramics for aeropropulsion use

J Eur Ceram Soc, 22 (2002), pp. 2757–2767

8. F. Monteverde, L. Scatteia

Resistance to thermal shock and to oxidation of metal diborides–SiC ceramics for aerospace application

J Am Ceram Soc, 90 (2007), pp. 1130–1138

9. X. Zhou, G.J. Zhang, Y. Li, Y. Kan, P. Wang

Hot pressed ZrB2–SiC–C ultra high temperature ceramics with polycarbosilane as a precursor

Mater Lett, 61 (2007), pp. 960–963

10. J.D. Bull, D.J. Rasky, C.C. Karika

Stability characterization of diboride composites under high velocity atmospheric flight conditions

Proceedings of the 24th international SAMPE technical conference (1992), pp. 1092–1106

11. M.M. Opeka, I.G. Talmy, E.J. Wuchina, J.A. Zaykoski, S.J. Causey

Mechanical, thermal, and oxidation properties of refractory hafnium and zirconium compounds

J Eur Ceram Soc, 19 (1999), pp. 2405–2414

12. F. Monteverde, A. Bellosi, S. Guicciardi

Processing and properties of zirconium diboride-based composites

J Eur Ceram Soc, 22 (2002), pp. 279–288

13. F. Monteverde, S. Guicciardi, A. Bellosi

Advances in microstructure and mechanical properties of zirconium diboride based ceramics

Mater Sci Eng A, 346 (2003), pp. 310–319

14. A.L. Chamberlain, W.G. Fahrenholtz, G.E. Hilmas, D.T. Ellerby

High-strength zirconium diboride-based ceramics

J Am Ceram Soc, 87 (2004), pp. 1170–1172

15. W.G. Fahrenholtz, G.E. Hilmas, A.L. Chamberlain, J.W. Zimmermann, B. Fahrenholtz

Processing and characterization of ZrB2-based ultra-high temperature monolithic and fibrous monolithic ceramics

J Mater Sci, 39 (2004), pp. 5951–5957

16. A. Bellosi, F. Monteverde, D. Sciti

Fast densification of ultra-high-temperature ceramics by spark plasma sintering

Int J Appl Ceram Technol, 3 (2006), pp. 32–40

17. A.L. Chamberlain, W.G. Fahrenholtz, G.E. Hilmas

Pressureless sintering of zirconium diboride

J Am Ceram Soc, 89 (2006), pp. 450–456

18. A. Rezaie, W.G. Fahrenholtz, G.E. Hilmas

Effect of hot pressing time and temperature on the microstructure and mechanical properties of ZrB2–SiC

J Mater Sci, 42 (2007), pp. 2735–2744

19. J.W. Zimmermann, G.E. Hilmas, W.G. Fahrenholtz, F. Monteverde, A. Bellosi

Fabrication and properties of reactively hot pressed ZrB2–SiC ceramics

J Eur Ceram Soc, 27 (2007), pp. 2729–2736

20. W.G. Fahrenholtz, G.E. Hilmas, S.C. Zhang, S. Zhu

Pressureless sintering of zirconium diboride: particle size and additive effects

J Am Ceram Soc, 91 (2008), pp. 1398–1404

21. R. Asthana, M. Singh

Joining of Zr-based ultra-high-temperature composites using Pd-based braze alloys

Scripta Mater, 61 (2009), pp. 257–260

22. F. Monteverde, A. Bellosi

Oxidation of ZrB2-based ceramics in dry air

J Electrochem Soc, 150 (2003), pp. B552–B559

23. M.M. Opeka, I.G. Talmy, J.A. Zaykoski

Oxidation-based materials selection for 2000 °C+ hypersonic aerosurfaces: theoretical considerations and historical experience

J Mater Sci, 39 (2004), pp. 5887–5904

24. W.G. Fahrenholtz

The ZrB2 volatility diagram

J Am Ceram Soc, 88 (2005), pp. 3509–3512

25. F. Monteverde

The thermal stability in air of hot-pressed diboride matrix composites for uses at ultra-high temperatures

Corros Sci, 47 (2005), pp. 2020–2033

26. W.G. Fahrenholtz

Thermodynamic analysis of ZrB2–SiC oxidation: formation of a siC-depleted region

J Am Ceram Soc, 90 (2007), pp. 143–148

27. F. Monteverde, R. Savino

Stability of ultra-high-temperature ZrB2–SiC ceramics under simulated atmospheric re-entry conditions

J Eur Ceram Soc, 27 (2007), pp. 4797–4805

28. A. Rezaie, W.G. Fahrenholtz, G.E. Hilmas

Evolution of structure during the oxidation of zirconium diboride–silicon carbide in air up to 1500 °C

J Eur Ceram Soc, 27 (2007), pp. 2495–2501

29. J.J. Meléndez-Martínez, A. Domínguez-Rodríguez, F. Monteverde, C. Melandri, G. De Portu

Characterisation and high temperature mechanical properties of zirconium boride-based materials

J Eur Ceram Soc, 22 (2002), pp. 2543–2549

30. W.G. Fahrenholtz, G.E. Hilmas, I.G. Talmy, J.A. Zaykoski

Refractory diborides of zirconium and hafnium

J Am Ceram Soc, 90 (2007), pp. 1347–1364

Figure captions

Figure 1. Microstructure of the as-received materials (BSE contrast). (A) ZrB2–20 vol.% SiC (ZS). (B) ZrB2–30 vol.% C–14 vol.% SiC (ZSC). (C and D) Longitudinal and traversal section of ZrB2–20 vol.% SiC–35 vol.% SCS fibers (ZSS).

Figure 2. Detail of the fiber and matrix in ZSS showing penny cracks in the matrix, perpendicular to the SiC fibers.

Figure 3. EDS map of a section perpendicular to the fibers in the ZSS composite. Zr, Si and C elemental maps are included.

Figure 4. Typical stress–displacement curves for ZS (left), ZSC (center) and ZSS (right) compression tests at room temperature. Tests for ZS and ZSC were run at two strain rates and in samples with and without polished external surface. Tests for ZSS material were run in samples with the SCS-9a fiber perpendicular and parallel to the compression axis. Vertical scale is logarithmic and curves are offset for ease of comparison

Figure 5. Fracture surface in ZS after high strength compression tests. (A) General view showing grain pullout in SiC, and transgranular fracture in ZrB2. (B) Detail at higher magnification, showing interganular small cracks

Figure 6. Typical stress–displacement curves for ZS, ZSC and ZSS at 1400 and 1550 °C. Note that for ZSS the scale is 1/10th of the scale for ZS and ZSC. Curves are offset for ease of comparison

Figure 7. Compressive strengths of ZS, ZSC, and ZSS as a function of temperature.

Figure 8. Microstructure of ZSS after compression at 1550 °C in the trasversal direction. (A) General view (SE contrast) and (B) detail of the fibers (BSE contrast).

Figure 9. ZS and ZSC compressive strength after oxidation in atmospheric air at 1400 °C.

Figure 10. EDS composition maps of ZS after oxidation for 1 h at 1400 °C (left) and of ZSC after oxidation for 24 h at 1400 °C.

Figure 11. (Left) Characteristic microstructure of ZSC samples after 24 h exposure to oxidizing atmosphere at 1400 °C. Several zones can be distinguished. (Right) Relevant EDS spectra obtained from the four zones depicted.

Figure 12. Evolution of the oxide layer thickness with exposure time for ZS (top) and ZSC (bottom). The data has been fitted to a $d \propto \sqrt{t + t_o}$ law which is characteristic of a diffusional process. For ZS, to≈0.

Figure 1

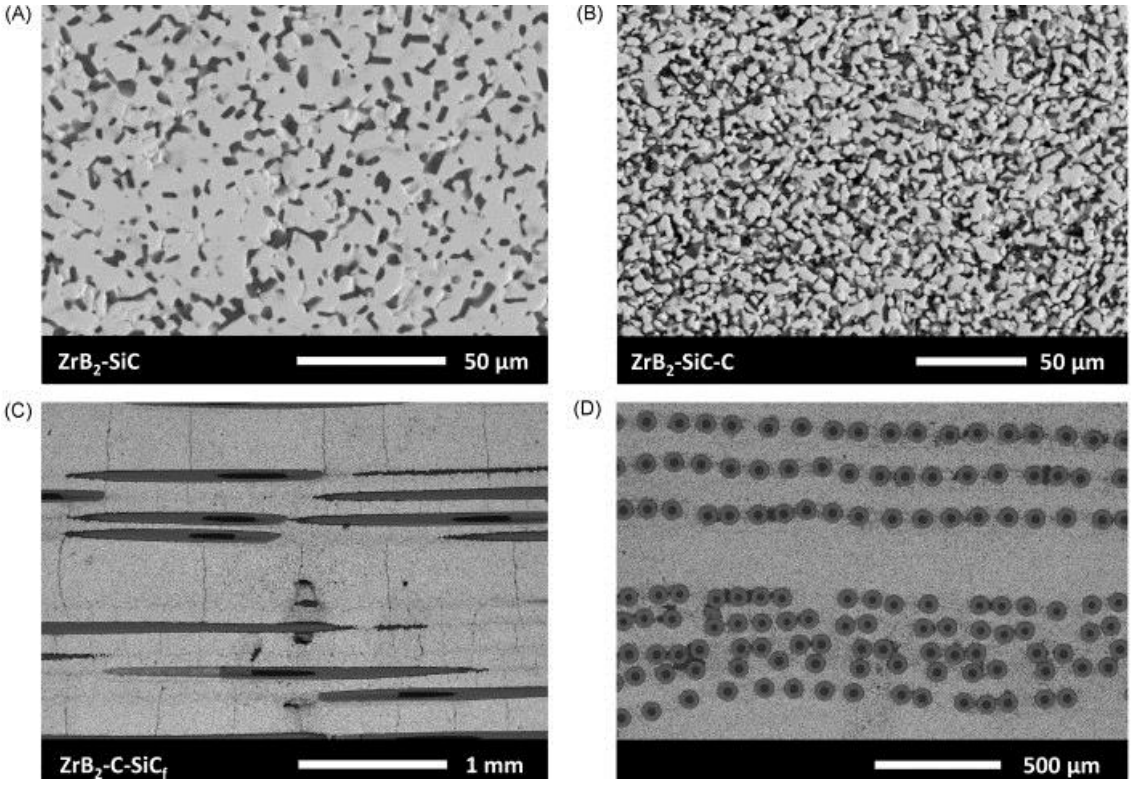

Figure 2

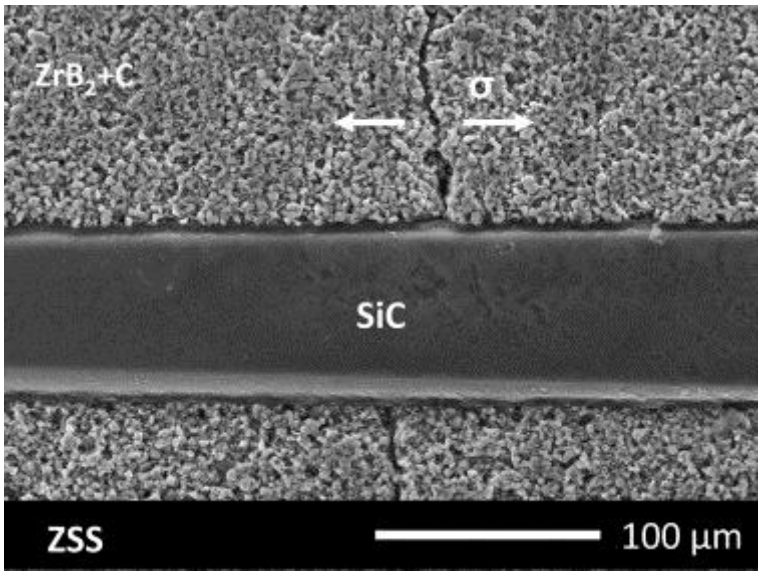

Figure 3

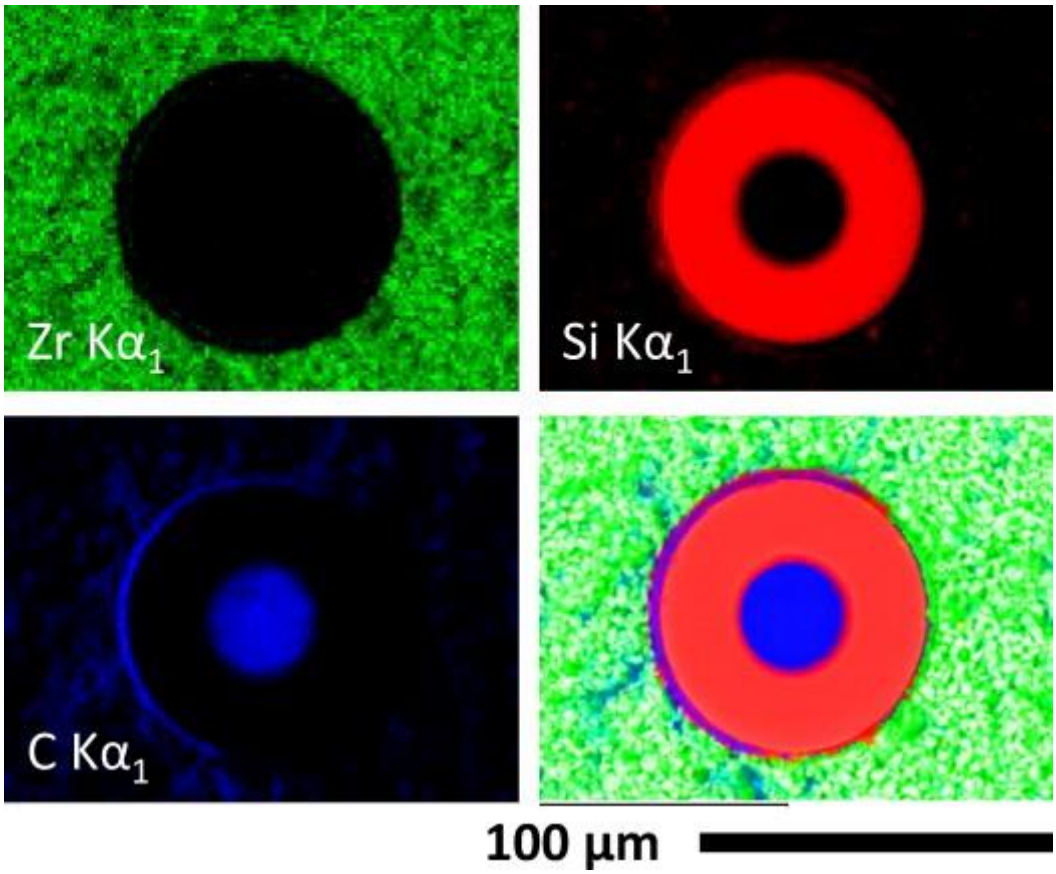

Figure 4

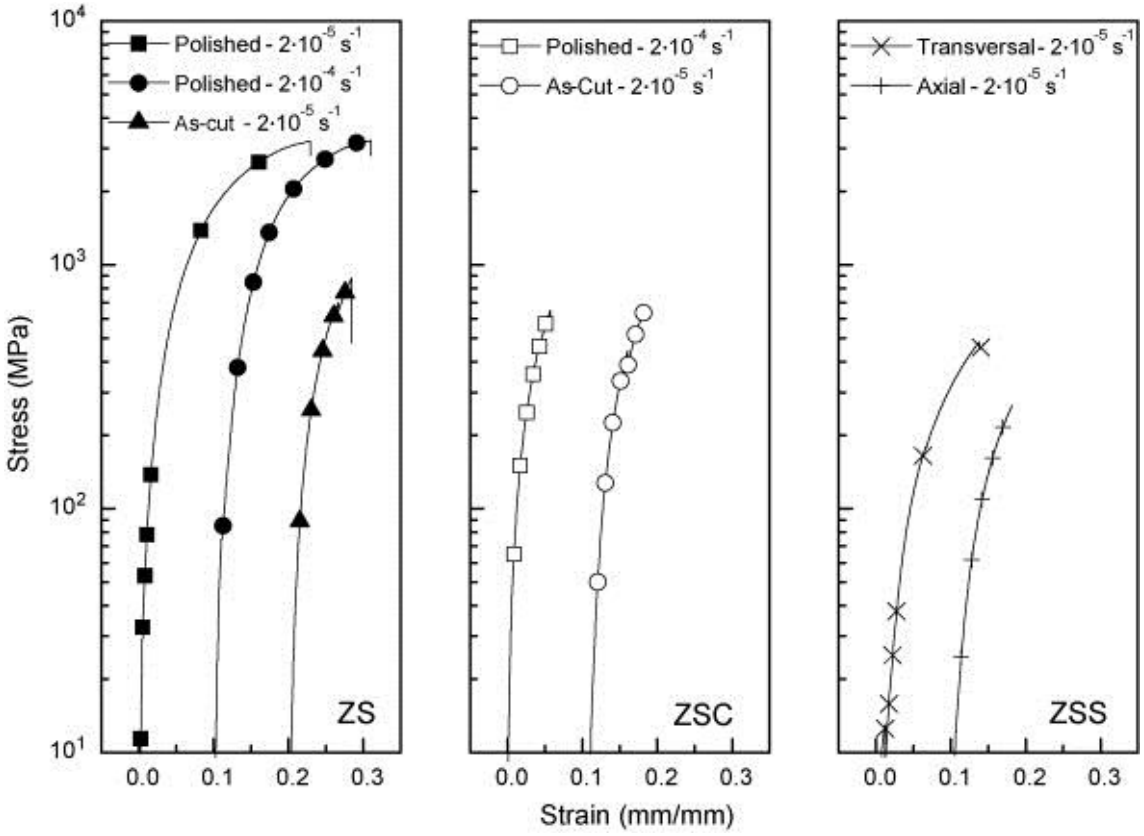
Polished - 2·10^-5 s^-1
Polished - 2·10^-4 s^-1
As-cut - 2·10^-5 s^-1
ZS
Polished - 2·10^-4 s^-1
As-Cut - 2·10^-5 s^-1
ZSC
Transversal - 2·10^-5 s^-1
Axial - 2·10^-5 s^-1
ZSS
Stress (MPa)
Strain (mm/mm)
10^4
10^3
10^2
10^1
0.0
0.1
0.2
0.3

Figure 5

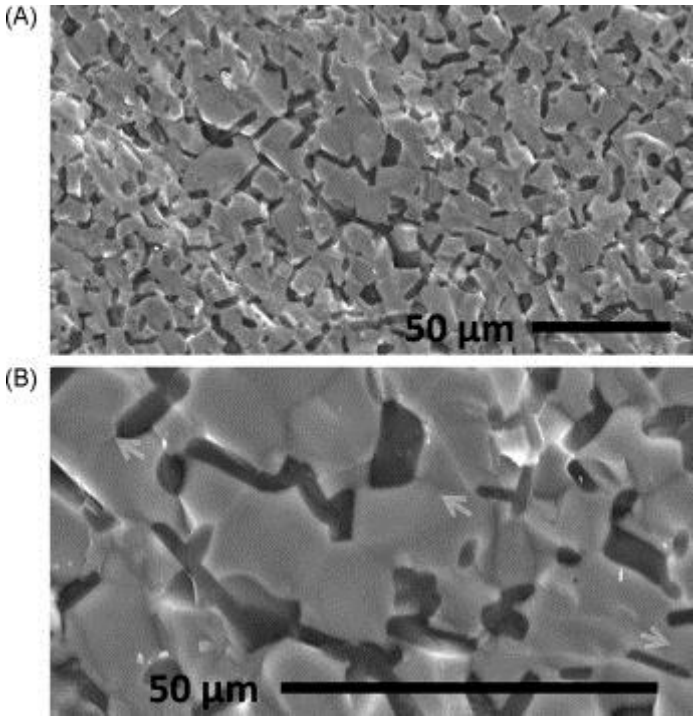

Figure 6

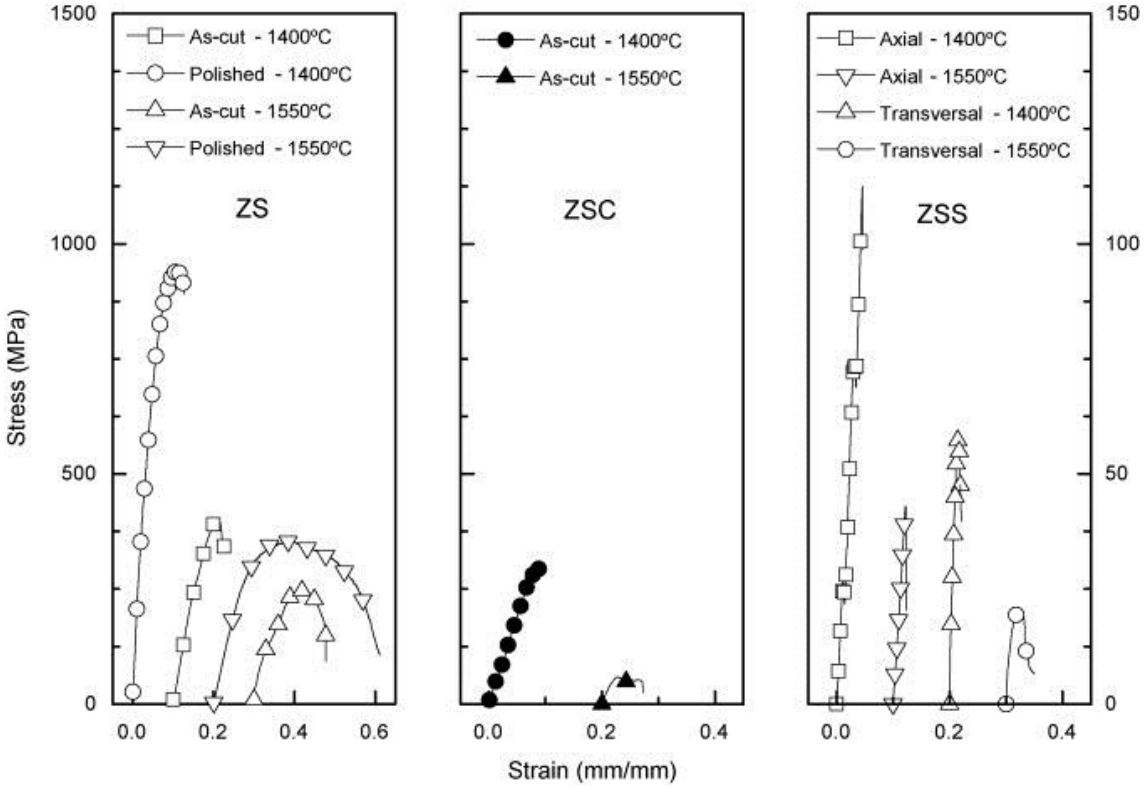
As-cut - 1400ºC
Polished - 1400ºC
As-cut - 1550ºC
Polished - 1550ºC
ZS
ZSC
Axial - 1400ºC
Axial - 1550ºC
Transversal - 1400ºC
Transversal - 1550ºC
ZSS
Stress (MPa)
Strain (mm/mm)
1500
1000
500
0
150
100
50
0.0
0.2
0.4
0.6

Figure 7

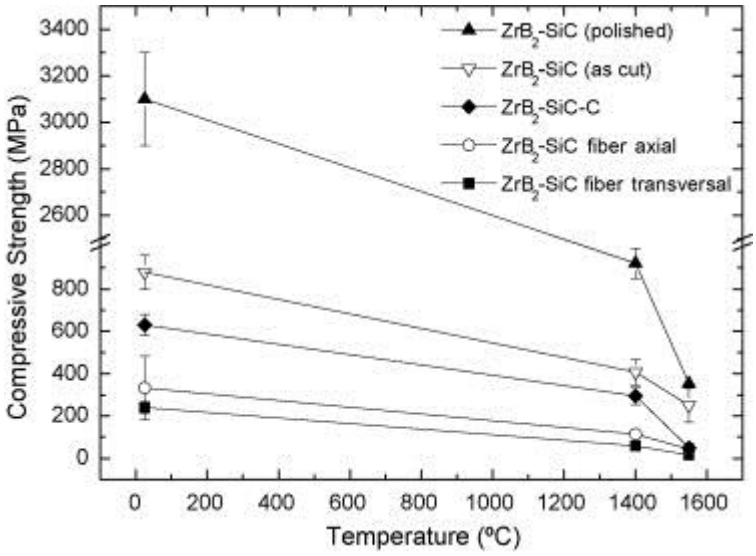
ZrB2-SiC (polished)
ZrB2-SiC (as cut)
ZrB2-SiC-C
ZrB2-SiC fiber axial
ZrB2-SiC fiber transversal
Compressive Strength (MPa)
Temperature (ºC)
3400
3200
3000
2800
2600
800
600
400
200
0
0
200
400
600
800
1000
1200
1400
1600

Figure 8

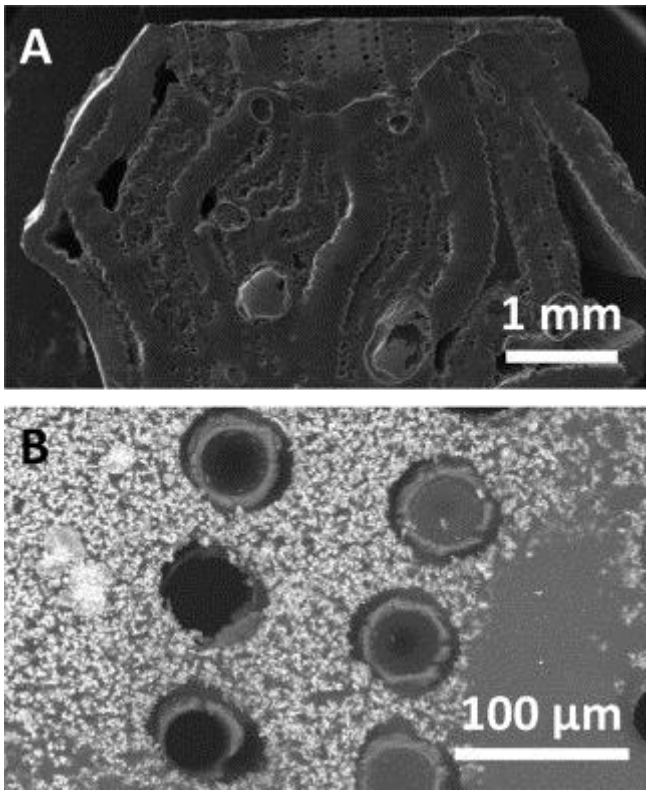

Figure 9

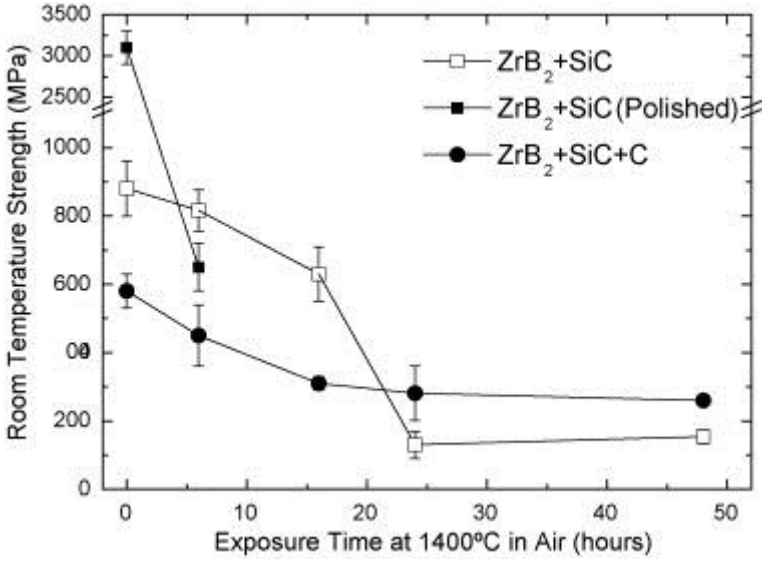
Room Temperature Strength (MPa)
Exposure Time at 1400ºC in Air (hours)
ZrB2+SiC
ZrB2+SiC (Polished)
ZrB2+SiC+C
3500
3000
2500
1000
800
600
200
0
0
10
20
30
40
50

Figure 10

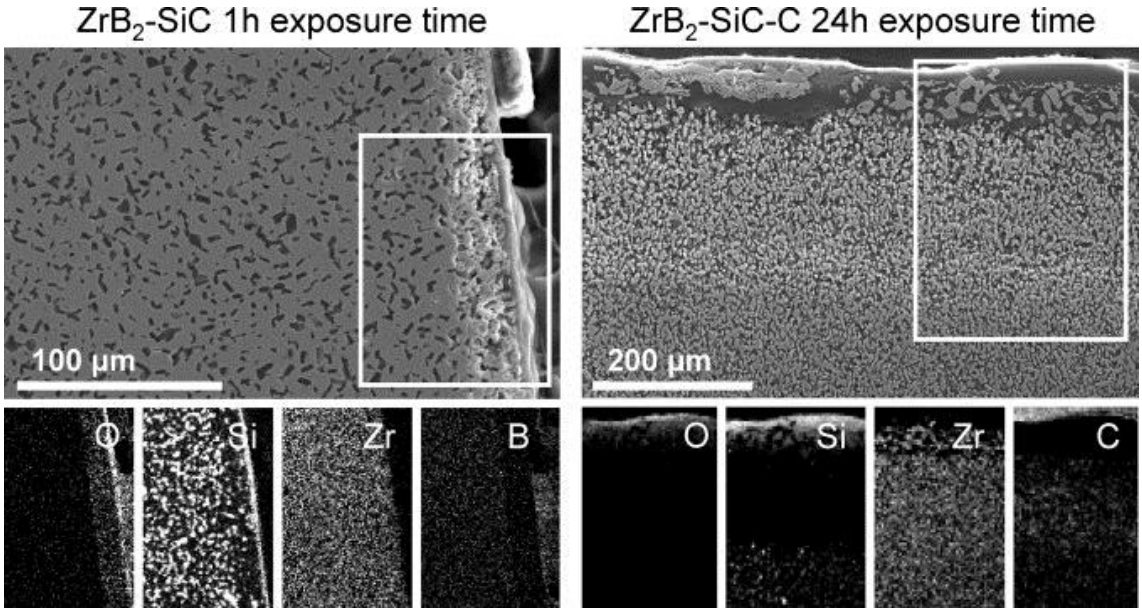
ZrB2-SiC 1h exposure time
ZrB2-SiC-C 24h exposure time
100 µm
200 µm
O
Si
Zr
B
O
Si
Zr
C

Figure 11

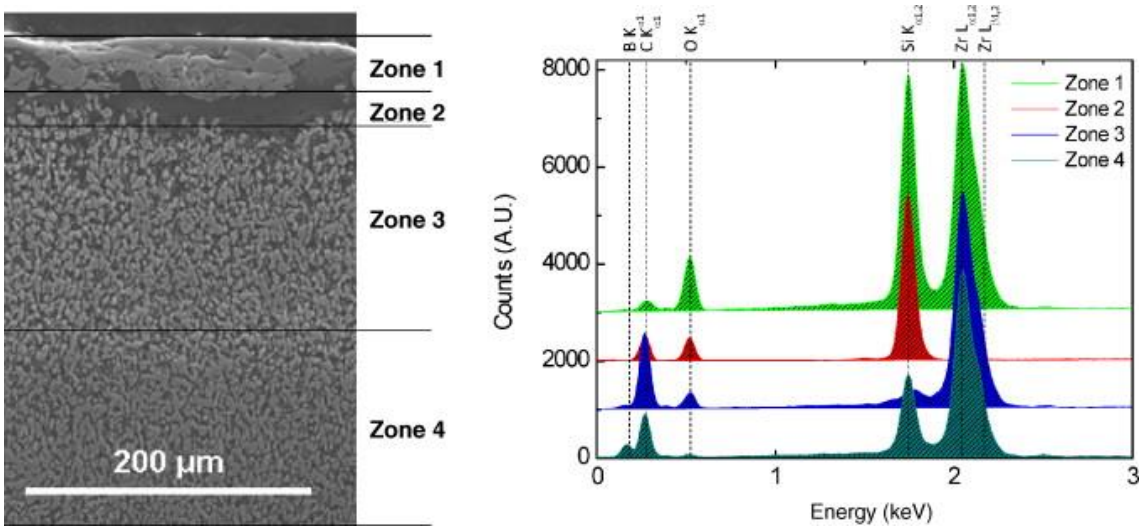
Zone 1
Zone 2
Zone 3
Zone 4
200 µm
B K
C K
O K
Si K
Zr L
Zr L
Zone 1
Zone 2
Zone 3
Zone 4
Counts (A.U.)
Energy (keV)
0
2000
4000
6000
8000
0
1
2
3

Figure 12

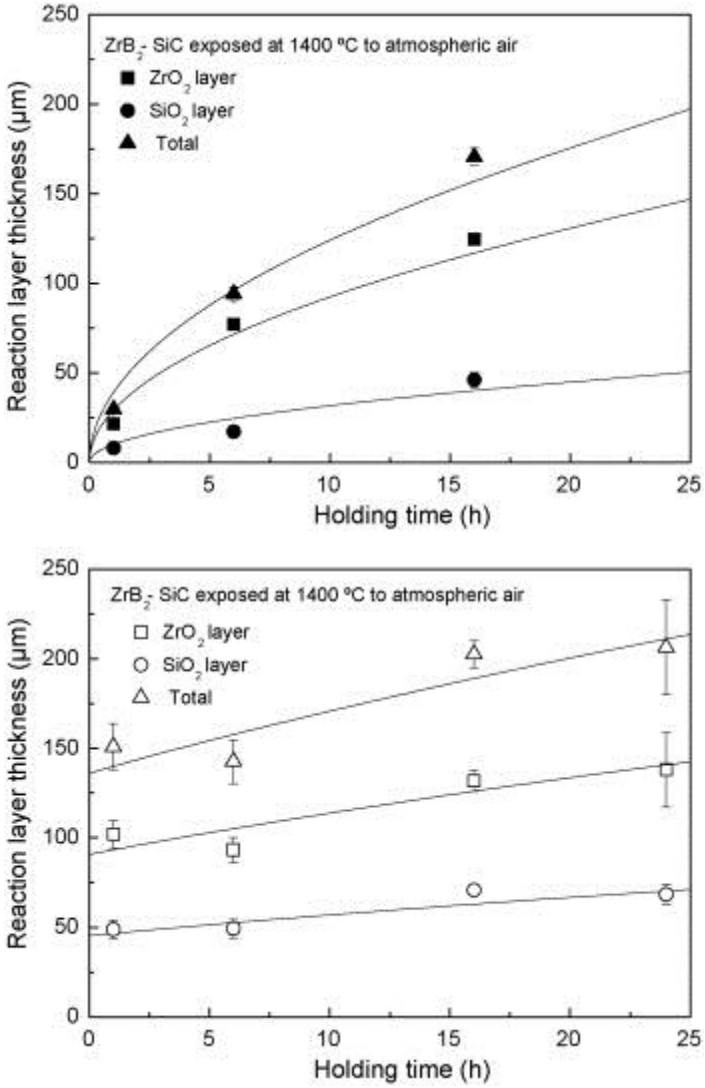
ZrB2- SiC exposed at 1400 ºC to atmospheric air
ZrO2 layer
SiO2 layer
Total
Reaction layer thickness (µm)
Holding time (h)
0
50
100
150
200
250
0
5
10
15
20
25

ZrB2- SiC exposed at 1400 ºC to atmospheric air
ZrO2 layer
SiO2 layer
Total
Reaction layer thickness (µm)
Holding time (h)
0
50
100
150
200
250
0
5
10
15
20
25